AJNR

Direct In Vivo MRI Discrimination of Brain Stem Nuclei and Pathways

T.M. Shepherd, B. Ades-Aron, M. Bruno, H.M. Schambra and M.J. Hoch

AJNR Am J Neuroradiol 2020, 41 (5) 777-784
doi: https://doi.org/10.3174/ajnr.A6542
http://www.ajnr.org/content/41/5/777

Direct In Vivo MRI Discrimination of Brain Stem Nuclei and Pathways

T.M. Shepherd, B. Ades-Aron, M. Bruno, H.M. Schambra, and M.J. Hoch

ABSTRACT

BACKGROUND AND PURPOSE: The brain stem is a complex configuration of small nuclei and pathways for motor, sensory, and autonomic control that are essential for life, yet internal brain stem anatomy is difficult to characterize in living subjects. We hypothesized that the 3D fast gray matter acquisition T1 inversion recovery sequence, which uses a short inversion time to suppress signal from white matter, could improve contrast resolution of brain stem pathways and nuclei with 3T MR imaging.

MATERIALS AND METHODS: After preliminary optimization for contrast resolution, the fast gray matter acquisition T1 inversion recovery sequence was performed in 10 healthy subjects (5 women; mean age, 28.8 ± 4.8 years) with the following parameters: TR/TE/TI = 3000/2.55/410 ms, flip angle = 4°, isotropic resolution = 0.8 mm, with 4 averages (acquired separately and averaged outside *k*-space to reduce motion; total scan time = 58 minutes). One subject returned for an additional 5-average study that was combined with a previous session to create a highest quality atlas for anatomic assignments. A 1-mm isotropic resolution, 12-minute version, proved successful in a patient with a prior infarct.

RESULTS: The fast gray matter acquisition T1 inversion recovery sequence generated excellent contrast resolution of small brain stem pathways in all 3 planes for all 10 subjects. Several nuclei could be resolved directly by image contrast alone or indirectly located due to bordering visualized structures (eg, locus coeruleus and pedunculopontine nucleus).

CONCLUSIONS: The fast gray matter acquisition T1 inversion recovery sequence has the potential to provide imaging correlates to clinical conditions that affect the brain stem, improve neurosurgical navigation, validate diffusion tractography of the brain stem, and generate a 3D atlas for automatic parcellation of specific brain stem structures.

ABBREVIATION: FGATIR = fast gray matter acquisition T1 inversion recovery

The human brain stem represents the complex interdigitation of compact anatomic pathways and nuclei that control or modulate motor, sensory, autonomic, and cognitive functions. Many brain stem structures are essential for survival.[1] Patients can experience profound symptoms and disability even from small focal brain stem lesions due to ischemic stroke, multiple sclerosis, infections, vascular malformations, or tumors.[2-6] Histopathologic changes in specific brain stem structures can lead to neurodegeneration associated with movement disorders, such as Parkinson disease, progressive supranuclear palsy, and multiple system atrophy.[7-11] Even with state-of-the-art clinical MR imaging, it remains challenging to confidently localize the spatial locations of specific brain stem structures or to detect early pathologic changes to these structures in individual patients before postmortem examination.

To estimate the location of a particular brain stem structure in current practice, clinicians triangulate on the basis of surface landmarks, limited MR imaging–visible internal features, and mental representations of histology-stained sections from the same superior-inferior level. Systematic dissections of normal cadaver brains may improve the accuracy of this qualitative approach, particularly

Received January 28, 2020; accepted after revision March 19.

From the Departments of Radiology (T.M.S., B.A.-A., M.B.), Electrical and Computer Engineering (B.A.-A.), and Neurology (H.M.S.), New York University, New York, New York; and Department of Radiology (M.J.H.), University of Pennsylvania, Philadelphia, Pennsylvania.

T.M.S. received research support from the National Institute of Aging (1K23 AG048622-01). HMS received research support from National Library of Medicine (R01LM013316) and National Institute of Neurological Disorders and Stroke (K02 NS104207). H.M.S., T.M.S., and B.A.-A. received research support from the National Institute of Neurological Disorders and Stroke (RO1 NS110696). This work was supported, in part, by the Center for Advanced Imaging Innovation and Research, a National Institutes of Health National Institute of Biomedical Technology resource center (grant P41EB017183).

Please address correspondence to Timothy Shepherd, MD, PhD, Department of Radiology, 660 First Ave, Room 226, New York, NY, 10016; e-mail: timothy.shepherd@nyumc.org; @tim0shepherd

Indicates open access to non-subscribers at www.ajnr.org
Indicates article with supplemental on-line photos.
Indicates article with supplemental on-line videos.

http://dx.doi.org/10.3174/ajnr.A6542

to better identify safe entry zones for surgical procedures of the brain stem.[12,13] However, this overall approach does not account for anatomic distortion that frequently occurs with pathology (ie, no one performs surgery on the normal brain stem). Unfortunately, most stereotactic imaging–based brain atlases have emphasized resolution of cortex, white matter, or specific functional neurosurgery targets within the diencephalon.[14-18] Detailed image-based parcellation for internal brain stem anatomy remains scant.[19,20] The widely used FreeSurfer (http://surfer.nmr.mgh.harvard.edu) parcellation provides a single atlas label for the *entire* brain stem, and the more recent brain stem substructures algorithm only divides the brain stem into "midbrain," "pons," and "medulla."[21-23]

High-field MR imaging of postmortem, isolated brain stem specimens reveals the potential for MR imaging contrast resolution of internal brain stem anatomy comparable with histology,[24-27] though external validity is limited because this requires 8+ hours of scanning-dissected, coil-optimized individual specimens that may have altered MR imaging properties due to fixation and the postmortem interval.[28,29] Improved internal brain stem contrast also can be obtained with in vivo MR imaging using 7T systems,[30-33] susceptibility mapping,[34,35] relaxometry,[30,35,36] or various representations/models of diffusion contrast.[37-39] Diffusion tractography approaches can putatively identify many internal pathways and features of the brain stem.[36,39] However, diffusion tractography is prone to spurious tract generation and true-positive segmentations are challenging to validate.[40] Furthermore, diffusion contrast is often altered by underlying pathology (unfortunately when identifying brain stem structures is most needed clinically).

Several groups have previously reported novel MR imaging sequences that manipulate T1 relaxation to suppress signal from white matter and maximize internal contrast within the thalamus and basal ganglia for direct targeting during functional neurosurgery.[41-46] These sequences have various acronyms, but perhaps the most relevant was fast gray matter acquisition T1 inversion recovery (FGATIR).[42] Optimization of image contrast by manipulation of MR imaging sequence parameters was described in detail previously—the key concept is suppression of signal from voxels that contain myelin, even if the tissue does not contain classic white matter bundles by histology (eg, individual thalamic nuclei). Here, we demonstrate the tremendous advantages of also applying this MR imaging contrast mechanism for the direct identification of many internal brain stem structures in individual living subjects.

MATERIALS AND METHODS

This study was compliant with the New York University institutional review board and requirements of the Health Insurance Portability and Accountability Act. The data that support the findings of this study are available from the corresponding author on reasonable request. Healthy adult volunteers were imaged using a 3T Magnetom Prisma scanner with a 64-channel head and neck coil (Siemens). The sequence used here differs minimally from the originally reported FGATIR MR imaging sequence,[42] or the more recent fluid and white matter suppression (FLAWS) component[43] of the updated MP2RAGE sequence.[44] For simplicity, we refer to the sequence used as FGATIR throughout the remainder of this report. For all experiments described below, parallel imaging was not used, the radiofrequency mode was "fast," and "prescan normalize" was used (per manufacturer). Complete protocol details will be provided to interested readers. We empirically developed a protocol to obtain excellent contrast and spatial resolution to discriminate brain stem structures as determined by consensus between 2 board-certified diagnostic neuroradiologists with expertise in brain stem neuroanatomy.

We first explored how to use signal averaging during image reconstruction to improve contrast resolution of brain stem structures using a 1-mm isotropic resolution sequence with the following parameters: TR/TE/TI = 3000/2.4/410 ms, nonselective 180° inversion pulse, flip angle = 6°, 256 × 256 matrix, 256-mm-square FOV, 160 × 1 mm sagittal slices, bandwidth = 320 Hz/pixel, time = 12 minutes 9 seconds per 1 average. Due to the relatively long scan time per signal average and potential for subtle-but-compounding motion artifacts, we compared obtaining 4 averages in *k*-space before Fourier image transformation (the standard approach to signal averaging) versus when 4 averages were obtained independently, reconstructed to image space, spatially coregistered using a 6-*df* rigid-body transform with FMRIB Linear Image Registration Tool (FLIRT; http://www.fmrib.ox.ac.uk/fsl/fslwiki/FLIRT), and finally averaged together. While there is a signal-to-noise penalty for not obtaining multiple averages in *k*-space before Fourier image transformation,[47] this approach (4 separate 12-minute 9- second scans versus a continuous scan time of 48 minutes 36 seconds) resulted in less image degradation from subtle head motion, even in cooperative, tolerant, and experienced volunteers.

Next, we compared contrast resolution between 1- and 0.8-mm isotropic resolution in which the latter sequence parameters were the following: TR/TE/TI = 3000/2.11/410 ms, nonselective 180° inversion pulse, flip angle = 6°, matrix = 288 × 288, FOV = 230 mm square, 192 × 0.8 mm sagittal slices, bandwidth = 460 Hz/pixel, time = 14 minutes 26 seconds per 1 average. The image quality and fine anatomic detail of the 0.8-mm isotropic resolution were preferred by both neuroradiologists. Then, a single subject underwent the 0.8-mm isotropic protocol in 2 separate sessions with 4 and 5 individual averages (57 minutes 44 seconds and 72 minutes 10 seconds, respectively). Within-session averages were coregistered using 6-*df* rigid-body transforms, and data between the 2 scan sessions were aligned using a 12-*df* affine transform. Individual averages were then combined sequentially to assess image-quality improvement with additional averages. The 9-average dataset was used for annotating the relevant brain stem anatomy in this report; however, 4 averages were more practical for multiple subjects and appeared to provide sufficient contrast resolution for most individual brain stem structures (per both neuroradiologists). Ten right-handed subjects (5 women, 28.8 ± 4.8 years of age, mean Edinburgh Handedness Inventory score = 86 ± 19) then were each imaged using 4 individual averages of the 0.8-mm FGATIR protocol to assess inter-subject variability in brain stem anatomy. Anatomic assignment of structures was determined by consensus between the 2 neuroradiologists using commonly available references and standard nomenclature.[48-50] Note that axial images were created parallel to the commissural plane, while coronal images were parallel to the rhomboid fossa (which is not orthogonal to the commissural plane) (On-line Fig 1). For all figures, please see the Table for the specific labeled structures.

Key summary of labels for multiplanar anatomic images of the brain stem (Figs 1–6 and On-line Fig 2)

Label	Structure	Label	Structure
1	Mammillary body	32	Principal inferior olivary nucleus
2	Cerebral peduncle	33	Glossopharyngeal nerve
3	Pallido- and corticonigral tracts	34	Medullary pyramid
4	Substantia nigra, pars reticularis	35	Olivocerebellar fibers
5	Substantia nigra, pars compacta	36	Area postrema
6	Oculomotor nerve	37	Spinal trigeminal nucleus
7	Red nucleus	38	Cuneate nucleus
8	Medial lemniscus	39	Central gray matter
9	Spinothalamic tract	40	Internal arcuate fibers and sensory decussation
10	Central tegmental tract	41	Spinocerebellar tracts
11	Periaqueductal gray	42	Cuneate fasciculus
12	Medial longitudinal fasciculus	43	Gracile fasciculus
13	Inferior colliculus	44	Pyramidal decussation
14	Lateral lemniscus	45	Subthalamic nucleus
15	Decussation of superior cerebellar peduncles	46	Dentatorubrothalamic tract
16	Superior cerebellar peduncles	47	Posterior perforated substance
17	Rubrospinal tract	48	Habenulopeduncular tract
18	Corticospinal tract	49	Gracile nucleus
19	Pontocerebellar fibers	50	Lateral geniculate nucleus
20	Pontine nuclei	51	Medial geniculate nucleus
21	Trigeminal nerve	52	Superior colliculus
22	Sensory and motor trigeminal nuclei	53	Posterior commissure
23	Internal genu of facial nerve	54	Commissure of superior colliculus
24	Superior olivary nucleus	55	Brachium of the inferior colliculus
25	Middle cerebellar peduncle	56	Obex
26	Vestibular nuclear complex	57	Interpeduncular nucleus
27	Abducens nucleus	58	Tectospinal tract
28	Facial nerve	59	Trochlear nucleus
29	Vestibulocochlear nerve	60	Mesencephalic reticular formation
30	Trapezoid body	61	Ventral trigeminothalamic tract
31	Inferior cerebellar peduncle		

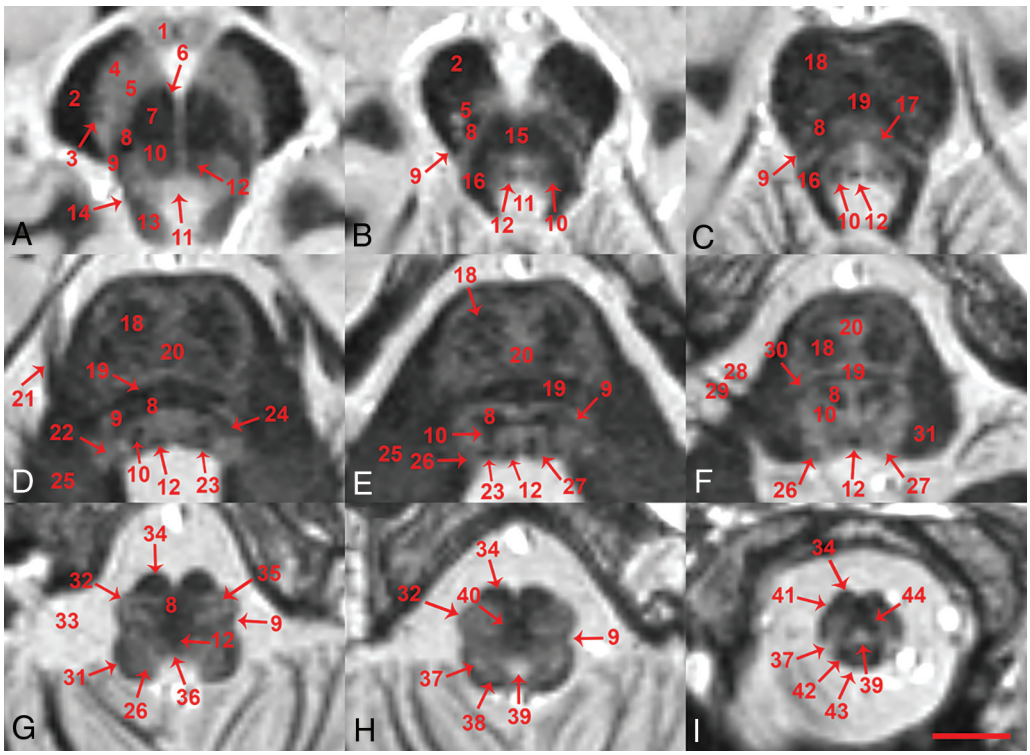

FIG 1. Superior-to-inferior axial in vivo MR images parallel to the intercommissural plane for the brain stem (number denotes the position below the plane), including the superior midbrain (*A*, 8.8 mm), inferior midbrain (*B*, 15.2 mm), midbrain-pons junction (*C*, 18.4 mm), superior midpons (*D*, 25.5 mm), inferior midpons (*E*, 29.5 mm), inferior pons (*F*, 35.9 mm), superior or "open" medulla (*G*, 43.1 mm), closed medulla at the sensory decussation (*H*, 47.1 mm) and motor decussation (*I*, 55.1 mm). A 26-year-old healthy control female subject, 0.8-mm isotropic resolution, 9 individual datasets coregistered and averaged, 2 imaging sessions with ~2-hour 15-minute total scan time (scale bar = 5 mm). Please see the Table and Results section for explanation of labeled structures.

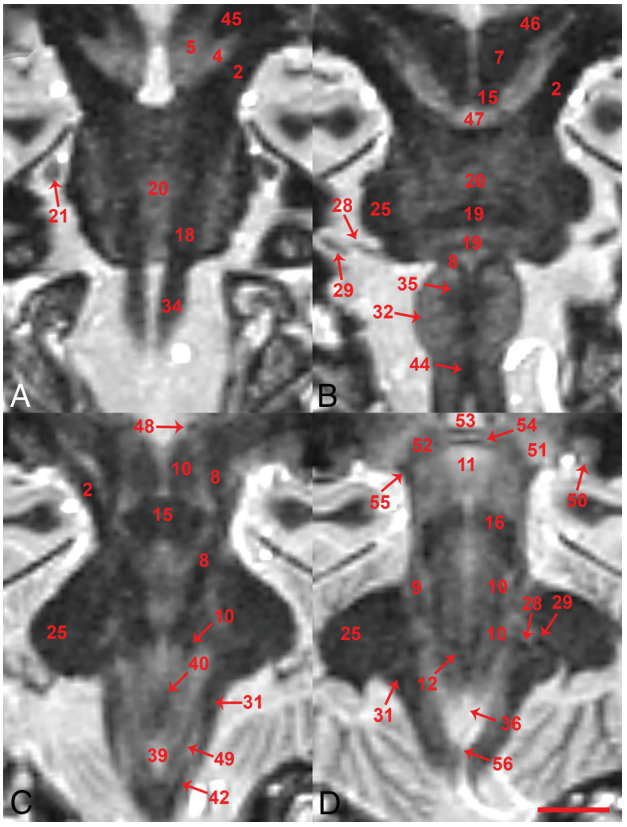

FIG 2. Anterior-to-posterior coronal in vivo MR images for the brain stem including 13.5-, 9-, 4.5-, and 1.5-mm anterior and parallel to the rhomboid fossa (*A–D*, respectively). A 26-year-old healthy control female subject, 0.8-mm isotropic resolution, 9 individual datasets coregistered and averaged, 2× imaging sessions, ~2-hour 15-minute total scan time (scale bar = 5 mm). Note this orientation is parallel to the long axis of the brain stem, but not orthogonal to the intercommissural plane. Please see the Table and the Results section for explanation of labeled structures.

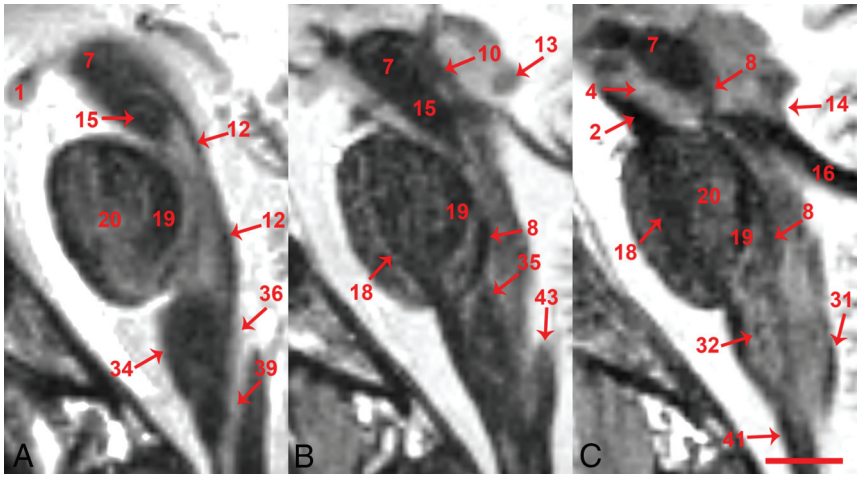

FIG 3. Medial-to-lateral sagittal in vivo MR images parallel to the interhemispheric plane and ventral medullary fissure for the brain stem including 1.2-, 2-, and 6-mm lateral to the midline (*A*, *B*, and *C*, respectively). A 26-year-old healthy control female subject, 0.8-mm isotropic resolution, 9 individual datasets coregistered and averaged, 2× imaging sessions, ~2-hour 15-minute total scan time (scale bar = 5 mm). Please see the Table and results section for explanation of labeled structures.

Finally, to demonstrate clinical feasibility, we performed a single average, 1-mm isotropic resolution FGATIR sequence (~12 minutes) in a patient with hemiplegia after ischemic stroke involving the corticospinal tract.

RESULTS

The FGATIR sequence provided novel MR imaging–derived contrast throughout the in vivo brain stem and allowed the direct identification of many small functionally important structures. Structure identification by 2 neuroradiologists was facilitated by 3-plane cross-referencing. Selected serial axial images illustrate contrast resolution of internal brain stem anatomy at canonical levels (Fig 1). Selected coronal and sagittal images also reveal excellent contrast resolution of internal brain stem anatomy (Figs 2 and 3, respectively). Such longitudinal images demonstrate the superior-inferior course of several brain stem pathways and the potential for the 0.8-mm isotropic FGATIR to enhance our understanding of the 3D organization of the brain stem. Videos of axial, coronal, and sagittal images through the brain stem are provided to interested readers on-line (On-line Videos 1–3).

Within the brain stem, the signal intensity or brightness of a specific structure appeared inversely correlated with the intensity of myelin staining in postmortem histology atlases.[48-50] Blood in the vertebral arteries and dural venous sinuses appeared the brightest. The next most hyperintense structures were CSF and adjacent gray matter such as the periaqueductal gray and area postrema, the latter a circumventricular organ with an altered extracellular matrix and vascular structure.[51,52] The third most hyperintense structures were more central gray matter within the brain stem such as the substantia nigra and pontine nuclei. Structures with intermediate hyperintensity were less compact or less densely myelinated structures like the inferior colliculi, central tegmental tract, and corticonigral pathways. Dark structures were classic myelinated brain stem pathways such as the medial longitudinal fasciculus, medial lemniscus, and pontocerebellar fibers. The darkest structures were densely myelinated pathways, including the medullary pyramids, superior/middle cerebellar peduncles, and larger cranial nerves. Cortical bone in the central skull base and the tectorial membrane also appeared very dark. Of note, the signal intensity (and shape) of the corticospinal tract varied along its course, appearing dark within the cerebral peduncles and medullary pyramids, but more diffuse and relatively brighter within the basis pontis. This appearance may represent interdigitation of pontine nuclei and pontocerebellar projections between white matter fascicles of the corticospinal tract.[48-50,53]

Labeling in the figures emphasizes unambiguous structures that can be identified well on the images. Most of these labeled structures are well-known to clinicians familiar with brain stem anatomy (eg, the medial

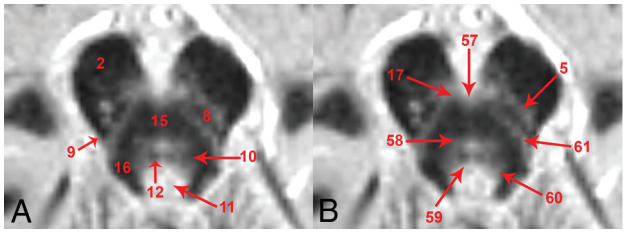

FIG 4. Direct, unambiguous identification of many myelinated structures in the inferior midbrain (*A*) also helps improve the spatial accuracy for indirect localization of bordering brain stem nuclei and pathways that are less densely myelinated at this level (*B*). The ventral trigeminothalamic tract[61] is located between the decussation of the superior cerebellar peduncles and medial lemniscus. Subtle dark bumps on the anterior and posterior aspects of the decussation[15] are consistent with the rubrospinal[17] and tectospinal tracts,[58] respectively. The bright midline structure anterolateral to the medial longitudinal fasciculus[8] should be the substantia nigra pars compacta.[5] The reticular formation[60] is the bright region posterolateral to the medial longitudinal fasciculus and central tegmental tract,[10] and anterolateral to the periaqueductal gray.[11] This region will also contain the locus coeruleus. The trochlear nucleus[59] should be along the posterior border of the medial longitudinal fasciculus. The interpeduncular nucleus[57] is off-midline anterior to the decussation of the superior cerebellar peduncles. Similar indirect localization can be derived at other brain stem levels, but is beyond the scope of this initial report.

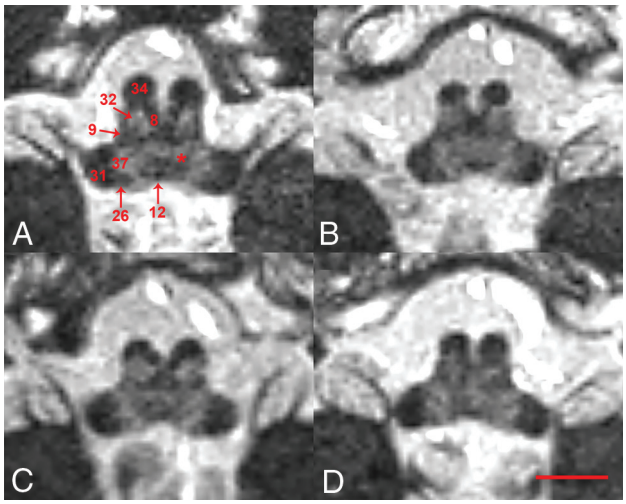

FIG 5. Axial in vivo MR images of the pontomedullary junction (superior to Fig 1*F*) selected from 4 different healthy adult controls (2 men) suggest reproducibility of overall image contrast across individuals and sexes (0.8-mm isotropic resolution, 4 averages, 58-minute total scan time, scale bar = 5 mm). The putative location of the pontomedullary reticular formation, a structure of interest for predicting limb function recovery after stroke, is denoted with an *asterisk*.

longitudinal fasciculus). Directly labeled visible structures also can be used to generate more exact indirect localization for other bordering internal brain stem structures. Figure 4 provides a highly detailed example of this approach for the inferior midbrain where the likely positions of multiple additional structures can be estimated relative to the borders and anatomic spaces formed between the medial longitudinal fasciculus, medial lemniscus, and decussation of the superior cerebellar peduncles. Annotation at this level of detail with descriptions of functional relevance is possible throughout the brain stem, but is beyond the scope of this initial report. Other selected examples of indirect localization that may be of general interest include the oculomotor complex (bright region posteromedial to the central tegmental tract in Fig 1*A*), pedunculopontine nucleus (bright region medial to the medial lemniscus and lateral to the decussation of the superior cerebellar peduncles, in Fig 1*B*), locus coeruleus (bright region posterior to the central tegmental tract and medial to the superior cerebellar peduncle in Fig 1*C*), and facial nucleus (bright region posterolateral to the central tegmental tract and medial to the cerebellar peduncles in Fig 1*F*). An inferior notch along the medial aspect of the left middle cerebellar peduncle with gray matter signal intensity in Fig 2*D* is the cochlear nucleus.

There also are subtle features in the images that are difficult to assign with certainty (and sometimes only visualized on 1 side) that likely correspond to specific structures better resolved with postmortem MR microscopy[53] and histology atlases.[48–50] Limited visualization may be from partial volume effects due to the small size of the structures relative to 0.8-mm isotropic voxels and/or less contrast relative to surrounding nervous tissue. On the right side of Fig 1*B*, there is an arc-like medially concave dark structure oriented anterior-posterior, consistent with the expected location of the left oculomotor nerve. In Fig 1*C*, *-D*, the tectospinal tract appears as a faint dark dotlike structure anterior to the medial lemniscus, particularly on the left side. In Fig 1*E*, the left tectospinal tract is more obvious, but there is marked asymmetry compared with the subject's right side. Also, in Fig 1*E*, the indistinct anterior margin of the medial lemniscus may represent the anteromedial continuation of the trapezoid body. In Fig 2*D*, an intermediate signal intensity line oriented inferomedial to superolateral, dividing the area postrema (on the right side of the image), may be the sulcus limitans. Some structures also are better recognized when the imaging plane is transverse to the structure. For example, the facial nerve in the lateral midpons is difficult to appreciate in the axial plane (Fig 1*F*), but better resolved in the coronal plane (Fig 2*D*).

The FGATIR images did not discriminate all brain stem structures well. It was not possible to distinguish the corticospinal tract from other white matter in the cerebral peduncle (Fig 1*A*). Boundaries of the medial lemniscus, tectospinal tract, and medial longitudinal fasciculus, which are adjacent to one another in an anterior-posterior orientation within the medulla, remain indistinct (Fig 1*G*). The inverse relationship of MR imaging signal intensity to white matter content described above also was not entirely consistent. For example, the red nucleus appeared isointense to enveloping cerebellorubral and cerebellothalamic fibers on MR imaging, but these structures are more distinct with classic white matter staining on histology.[48,49]

Contrast discrimination of structures improved with more signal averages for the FGATIR sequence with 0.8-mm isotropic resolution, but subjectively yielded less improvement beyond 4 averages (On-line Fig 2). Thus, a 4-average protocol was used to image 10 healthy volunteers (~1-hour scan time) to assess individual variability in contrast (Fig 5). We observed subtle differences in morphology (eg, compare the medullary pyramids in *A* and *C*) or contrast resolution (eg, compare sensory decussation in *A* and *D*), but the overall contrast and the structures observed appeared consistent across individuals. In some subjects, the

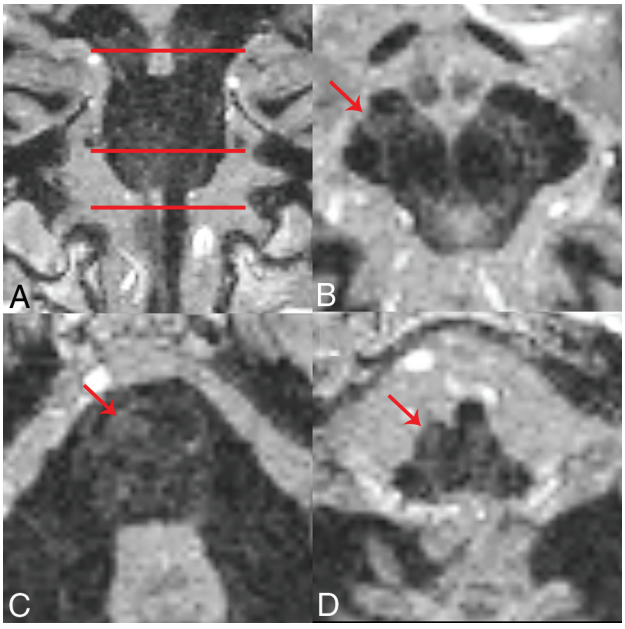

FIG 6. Example of the 1-mm isotropic resolution FGATIR sequence obtained in a 53-year-old woman with a remote prior right middle cerebral artery infarct involving the posterior frontoinsular cortex and subjacent basal ganglia (not shown). *A*, The axial planes for *B*–*D*. There is asymmetric absence of the compact dark corticospinal tract (*red arrows*) in the middle third of the right cerebral peduncle of the midbrain (*B*), right central basis pontis (*C*), and right medullary pyramid (*D*). These images appear very similar to myelin-stained histology changes of the brain stem after chronic right-sided infarct published in a popular neuroanatomy atlas.[48] This clinical example illustrates the feasibility of detecting brain stem pathology in patients using the faster, but lower 1-mm isotropic spatial resolution.

corticospinal tract signal intensity appeared asymmetrically darker on the left within the basis pontis (eg, Fig 1*E*). A similar observation has been reported in postmortem T2-weighted MR imaging microscopy of brain stems.[54]

To demonstrate clinical feasibility, we used the 1-average, 1-mm isotropic FGATIR (theoretically increasing available intravoxel signal by ~95%) to obtain images in a consented patient with prior right-sided infarct (Fig 6). Here we observed loss of the normal right corticospinal tract signal intensity in the cerebral peduncle and basis pontis, with complete absence of the right medullary pyramid. These findings were spatially remote from the site of ischemic stroke (right basal ganglia and internal capsule) and consistent with trans-synaptic degeneration of the tract.

DISCUSSION

Better discrimination of internal brain stem anatomy is critical for building knowledge about brain stem structure-function relationships in health, normal aging, and disease.[3,7,8] In current clinical practice, however, brain stem structure location can only be inferred indirectly on axial MR images on the basis of a priori knowledge of anatomy derived from histology (or postmortem MR microscopy), the superior-inferior position and surface landmarks, and limited internal contrast on clinical MR imaging. Current research atlases for imaging data like FreeSurfer[22,23] provide limited detail for the internal brain stem anatomy. Here, we identified brain stem anatomy using the FGATIR sequence, which uses a short inversion time to suppress signal from myelin. Previous groups using FGATIR (or similar contrast) emphasized applications for whole-brain segmentation or identification of diencephalic and spinal cord structures.[41-46] FGATIR not only enables the direct visualization of brain stem structures, but also the brain stem structures identified can be used for more precise indirect localization of additional bordering brain stem structures (eg, Fig 4). Internal brain stem contrast can be generated directly using FGATIR without the need for postprocessing, modeling assumptions, or ultra-high-field MR imaging systems. Contrast was consistent across multiple subjects and was feasible to obtain in patients with stroke.

Other MR imaging methods have provided some contrast resolution of internal brain stem anatomy, but are clinically or technically limited. Submillimeter isotropic resolution MR microscopy images can be obtained from isolated postmortem brain stem samples;[24-27] however, these protocols required 8–200 hours of scanning using ultra-high-field magnets and radiofrequency coils smaller than the human head, making this approach impractical for living subjects. Maps of diffusion parameters and tractography provide improved contrast resolution of internal brain stem anatomy.[36,39] However, diffusion MR imaging resolution of submillimeter brain stem pathways is challenging in vivo due to signal-to-noise limitations. Reliance on high-resolution diffusion MR imaging for anatomic localization can also be problematic due to inherent geometric distortion, particularly in structures near the skull base, and results in spatial misregistration with volumetric sequences. Unlike FGATIR, diffusion MR imaging contrast depends on complex mathematic representations or models that have proved challenging to validate in vivo.[40] FGATIR may provide complementary contrast for validating brain stem diffusion tractography or for independently extracting diffusion values from brain stem structures/regions. Joint reconstruction of multiple MR imaging contrasts, including FGATIR, may provide the best contrast resolution of brain stem anatomy.[55]

The 1-mm isotropic FGATIR acquisition with 1 average (~12- minute acquisition) is a relatively long acquisition for clinical MR imaging protocols, but appears feasible in patients (Fig 6), particularly in specific clinical circumstances that justify such a long scan. For example, the FGATIR sequence was originally developed for functional neurosurgery to improve deep brain stimulator electrode placement within the subthalamic nucleus.[42] We plan to implement FGATIR in clinical patients to better localize specific brain stem structures affected by focal lesions (eg, infarcts, demyelinating, or inflammatory lesions). This sequence also may prove helpful for planning surgical biopsies or anatomic corridors for tumor resection.[12,13] The 800-μm isotropic data require 3–4 averages for useful contrast resolution, which may be susceptible to motion-related image degradation in noncompliant individuals. This concern may be addressed by applying several recently developed methods to accelerate FGATIR acquisitions, including sliding window reconstructions of *k*-space,[56] compressed sensing image reconstruction of undersampled data,[57] and deep learning approaches to improve suboptimal image contrast produced by shortened scan times.[58,59] Clinical feasibility also can be supported through the use of a diffeomorphic template for coregistration of limited contrast

FGATIR images from individual patients[60] or by training a neural network to recognize small brain stem structures with limited FGATIR contrast.[58]

Using FGATIR to depict brain stem anatomy has other potential limitations. Not all brain stem structures were directly resolved by FGATIR. We identified brain stem structures on the basis of correspondences to labeled myelin-stained histology images in published atlases,[48-50] but direct structure-function correlations in the same brain would be helpful. Like diffusion MR imaging, FGATIR image contrast in the brain stem also could change with aging or disease. Such changes occur in other non-diffusion-weighted scans of the brain stem such as neuromelanin MR imaging in subjects with Parkinson disease.[61] In our ongoing work, FGATIR-based contrast in older patients with stroke and essential tremor appears similar to that in age-matched healthy controls and younger subjects (unpublished data). However, the effects of aging and disease on FGATIR contrast require systematic investigation.

To date, the teaching, clinical targeting, and research of brain stem structures have largely relied on neuroanatomic atlases that have limitations. Most brain stem plates in the Haines atlas are from a single individual with trans-synaptic degeneration of the corticospinal tract due to internal capsule infarction.[48] The Schaltenbrand brain atlas, widely used for functional neurosurgery in the United States, relies predominately on 3 thalami of different sizes and limited spatial overlap.[62] This atlas also provided annotated images of only 1 brain stem in the axial plane.[17] MR imaging data with FGATIR contrast have some advantages over traditional neuroanatomy atlases that use postmortem histology. First, the 3D imaging datasets enable simultaneous localization and visualization of specific structures in multiple planes. Depiction of brain stem anatomy is not limited to the plane of section like histologic sampling, and specific oblique image reconstructions can be obtained to emphasize certain key spatial relationships. Second, collections of MR imaging data are less expensive and less time-intensive, providing greater opportunity to characterize brain stem structure variations across multiple individual brains. We intend to collect FGATIR data from a large cohort of subjects to create a diffeomorphic template with atlas labels[60,63,64] for the human brain stem. These data could be used to investigate size and shape differences in the brain stem and as an independent method for extracting quantitative data from MR imaging and PET data in future investigations of small brain stem structure changes associated with aging and different diseases.[65,66]

CONCLUSIONS

The FGATIR sequence provided excellent novel contrast resolution of internal brain stem pathways and nuclei at 3T in healthy living subjects. The 1-mm isotropic resolution protocol was clinically feasible (~12-minute acquisition) and may immediately help with structure-function correlations or surgical corridor planning in the brain stem for individual patients. The FGATIR sequence also provided image contrast that may be helpful to complement and/or validate other advanced MR imaging methods for brain stem anatomy such as diffusion tractography.

Disclosures: Timothy M. Shepherd—*UNRELATED: Stock/Stock Options:* MICroStructure Imaging. Heidi M. Schambra—*RELATED: Grant:* National Institutes of Health, *Comments:* grant R01 NS110696*; *UNRELATED: Grants/Grants Pending:* National Institutes of Health.* *Money paid to the institution.

REFERENCES

1. Carpenter MB, Strong OS, Truex RC. *Human Neuroanatomy (Formerly Strong and Elwyn's Human Neuroanatomy)*. 7th ed. Lippincott Williams & Wilkins; 1976
2. Ortiz de Mendivil A, Alcalá-Galiano A, Ochoa M, et al. **Brainstem stroke: anatomy, clinical and radiological findings.** *Semin Ultrasound CT MR* 2013;34:131–41 CrossRef Medline
3. Tintore M, Rovira A, Arrambide G, et al. **Brainstem lesions in clinically isolated syndromes.** *Neurology* 2010;75:1933–38 CrossRef Medline
4. Tan IL, Mowry EM, Steele S, et al. **Brain stem encephalitis: etiologies, treatment, and predictors of outcome.** *J Neurol* 2013;260:2312–19 CrossRef Medline
5. Han SJ, Englot DJ, Kim H, et al. **Brainstem arteriovenous malformations: anatomical subtypes, assessment of "occlusion in situ" technique, and microsurgical results.** *J Neurosurg* 2015;122:107–17 CrossRef Medline
6. Donaldson SS, Laningham F, Fisher PG. **Advances toward an understanding of brainstem gliomas.** *J Clin Oncol* 2006;24:1266–72 CrossRef Medline
7. Dickson DW. **Parkinson's disease and parkinsonism: neuropathology.** *Cold Spring Harb Perspect Med* 2012;2 CrossRef Medline
8. Seidel K, Mahlke J, Siswanto S, et al. **The brainstem pathologies of Parkinson's disease and dementia with Lewy bodies.** *Brain Pathol* 2015;25:121–35 CrossRef Medline
9. Dugger BN, Tu M, Murray ME, et al. **Disease specificity and pathologic progression of tau pathology in brain stem nuclei of Alzheimer's disease and progressive supranuclear palsy.** *Neurosci Lett* 2011;491:122–26 CrossRef Medline
10. Santpere G, Ferrer I. **Delineation of early changes in cases with progressive supranuclear palsy-like pathology: astrocytes in striatum are primary targets of tau phosphorylation and GFAP oxidation.** *Brain Pathol* 2009;19:177–87 CrossRef Medline
11. Brettschneider J, Irwin DJ, Boluda S, et al. **Progression of alpha-synuclein pathology in multiple system atrophy of the cerebellar type.** *Neuropathol Appl Neurobiol* 2017;43:315–29 CrossRef Medline
12. Yagmurlu K, Rhoton AL Jr, Tanriover N, et al. **Three-dimensional microsurgical anatomy and the safe entry zones of the brainstem.** *Neurosurgery* 2014;(Suppl 4):602–19; discussion 619–20 CrossRef Medline
13. Martinez JA, de Oliveira E, Tedeschi H, et al. **Microsurgical anatomy of the brain stem.** *Operative Techniques in Neurosurgery* 2000;3:80–86 CrossRef
14. Talairach J, Tournoux P. *Co-Planar Stereotaxic Atlas of the Human Brain: 3-Dimensional Proportional System—An Approach to Cerebral Imaging*. Thieme Medical Publishers; 1988
15. Talairach J, Tournoux P, Missir O. *Referentially Oriented Cerebral MRI Anatomy: An Atlas of Stereotaxic Anatomical Correlations for Gray and White Matter*. Thieme Verlag; 1993
16. Ono M, Abernathey CD, Kubik S. *Atlas of the Cerebral Sulci*. Thieme; 1990
17. Schaltenbrand G, Hassler R, Wahren W. *Atlas of Stereotaxy of the Human Brain*. 2nd ed. Thieme; 1997
18. Cohn MC, Hudgins PA, Sheppard SK, et al. **Pre- and postoperative MR evaluation of stereotactic pallidotomy.** *AJNR Am J Neuroradiol* 1998;19:1075–80 Medline
19. Niemann K, van den Boom R, Haeselbarth K, et al. **A brainstem stereotactic atlas in a three-dimensional magnetic resonance imaging navigation system: first experiences with atlas-to-patient registration.** *J Neurosurg* 1999;90:891–901 CrossRef Medline
20. Afshar F, Watkins S, Yap JC. *Stereotaxic Atlas of the Human Brainstem and Cerebellar Nuclei: A Variability Study*. Raven Press; 1978
21. Fischl B. **FreeSurfer.** *Neuroimage* 2012;62:774–81 CrossRef Medline
22. Iglesias JE, Van Leemput K, Bhatt P, et al; Alzheimer's Disease Neuroimaging Initiative. **Bayesian segmentation of brainstem structures in MRI.** *Neuroimage* 2015;113:184–95 CrossRef Medline

23. FreeSurfer. http://surfer.nmr.mgh.harvard.edu/. Accessed September 24, 2019
24. Aggarwal M, Zhang J, Pletnikova O, et al. **Feasibility of creating a high-resolution 3D diffusion tensor imaging based atlas of the human brainstem: a case study at 11.7 T.** *Neuroimage* 2013;74:117–27 CrossRef Medline
25. Soria G, De Notaris M, Tudela R, et al. **Improved assessment of ex vivo brainstem neuroanatomy with high-resolution MRI and DTI at 7 Tesla.** *Anat Rec (Hoboken)* 2011;294:1035–44 CrossRef Medline
26. Calabrese E, Hickey P, Hulette C, et al. **Postmortem diffusion MRI of the human brainstem and thalamus for deep brain stimulator electrode localization.** *Hum Brain Mapp* 2015;36:3167–78 CrossRef Medline
27. Naidich T, Castillo M, Cha S, et al. *Imaging of the Brain*. Saunders; 2012
28. Shepherd TM, Thelwall PE, Stanisz GJ, et al. **Aldehyde fixative solutions alter the water relaxation and diffusion properties of nervous tissue.** *Magn Reson Med* 2009;62:26–34 CrossRef Medline
29. Shepherd TM, Flint JJ, Thelwall PE, et al. **Postmortem interval alters the water relaxation and diffusion properties of rat nervous tissue: implications for MRI studies of human autopsy samples.** *Neuroimage* 2009;44:820–26 CrossRef Medline
30. Deistung A, Schäfer A, Schweser F, et al. **High-resolution MR imaging of the human brain stem in vivo at 7 Tesla.** *Front Hum Neurosci* 2013;7:710 CrossRef Medline
31. Gizewski ER, Maderwald S, Linn J, et al. **High-resolution anatomy of the human brain stem using 7-T MRI: improved detection of inner structures and nerves?** *Neuroradiology* 2014;56:177–86 CrossRef Medline
32. Cho ZH, Calamante F, Chi JG. *7.0 Tesla MRI Brain White Matter Atlas*. 2nd ed. Springer-Verlag; 2015
33. Eapen M, Zald DH, Gatenby JC, et al. **Using high-resolution MR imaging at 7T to evaluate the anatomy of the midbrain dopaminergic system.** *AJNR Am J Neuroradiol* 2011;32:688–94 CrossRef Medline
34. Manova ES, Habib CA, Boikov AS, et al. **Characterizing the mesencephalon using susceptibility-weighted imaging.** *AJNR Am J Neuroradiol* 2009;30:569–74 CrossRef Medline
35. Hashido T, Saito S. **Quantitative T1, T2, and T2* mapping and semiquantitative neuromelanin-sensitive magnetic resonance imaging of the human midbrain.** *PLoS One* 2016;11:e0165160 CrossRef Medline
36. Hoch MJ, Chung S, Ben-Eliezer N, et al. **New clinically feasible 3T MRI protocol to discriminate internal brain stem anatomy.** *AJNR Am J Neuroradiol* 2016;37:1058–65 CrossRef Medline
37. Naganawa S, Yamazaki M, Kawai H, et al. **Anatomical details of the brainstem and cranial nerves visualized by high resolution readout-segmented multi-shot echo-planar diffusion-weighted images using unidirectional MPG at 3 T.** *Magn Reson Med Sci* 2011;10:269–75 CrossRef Medline
38. Nagae-Poetscher LM, Jiang H, Wakana S, et al. **High-resolution diffusion tensor imaging of the brain stem at 3 T.** *AJNR Am J Neuroradiol* 2004;25:1325–30 Medline
39. Habas C, Cabanis EA. **Anatomical parcellation of the brainstem and cerebellar white matter: a preliminary probabilistic tractography study at 3 T.** *Neuroradiology* 2007;49:849–63 CrossRef Medline
40. Maier-Hein KH, Neher PF, Houde JC, et al. **The challenge of mapping the human connectome based on diffusion tractography.** *Nat Commun* 2017;8:1349 CrossRef Medline
41. Reich CA, Hudgins PA, Sheppard SK, et al. **A high-resolution fast spin-echo inversion-recovery sequence for preoperative localization of the internal globus pallidus.** *AJNR Am J Neuroradiol* 2000;21:928–31 Medline
42. Sudhyadhom A, Haq IU, Foote KD, et al. **A high resolution and high contrast MRI for differentiation of subcortical structures for DBS targeting: the fast gray matter acquisition t1 inversion recovery (FGATIR).** *Neuroimage* 2009;47(Suppl 2);T44–52 CrossRef Medline
43. Tanner M, Gambarota G, Kober T, et al. **Fluid and white matter suppression with the MP2RAGE sequence.** *J Magn Reson Imaging* 2012;35:1063–70 CrossRef Medline
44. Marques JP, Gruetter R. **New developments and applications of the MP2RAGE sequence: focusing the contrast and high spatial resolution R1 mapping.** *PLoS One* 2013;8:e69294 CrossRef Medline
45. Tourdias T, Saranathan M, Levesque IR, et al. **Visualization of intrathalamic nuclei with optimized white-matter-nulled MPRAGE at 7T.** *Neuroimage* 2014;84:534–45 CrossRef Medline
46. Zerroug A, Gabrillargues J, Coll G, et al. **Personalized mapping of the deep brain with a white matter attenuated inversion recovery (WAIR) sequence at 1.5-Tesla: experience based on a series of 156 patients.** *Neurochirurgie* 2016;62:183–89 CrossRef Medline
47. Mitchell DG, Cohen MS. *MRI Principles*. 2nd ed. Saunders; 2004
48. Haines DE. *Neuroanatomy: An Atlas of Structures, Sections and Systems*. 6th ed. Lippincott Williams & Wilkins; 2004
49. DeArmond SJ, Fusco MM, Dewey MM. *Structure of the Human Brain: A Photographic Atlas*. 3rd ed. Oxford University Press; 1989
50. Warner JJ, Samuels MS. *Atlas of Neuroanatomy: With Systems Organization and Case Correlations*. Butterworth-Heinemann; 2001
51. Pócsai K, Kálmán M. **Extracellular matrix components mark the territories of circumventricular organs.** *Neurosci Lett* 2014;566:36–41 CrossRef Medline
52. Duvernoy HM, Risold PY. **The circumventricular organs: an atlas of comparative anatomy and vascularization.** *Brain Res Rev* 2007;56:119–47 CrossRef Medline
53. Naidich TP, Duvernoy HM, Delman BN, et al. *Duvernoy's Atlas of the Human Brain Stem and Cerebellum*. Springer-Verlag, Vienna; 2009
54. Hoch MJ, Bruno MT, Faustin A, et al. **3T MRI whole-brain microscopy discrimination of subcortical anatomy, Part 1: brain stem.** *AJNR Am J Neuroradiol* 2019;40:401–07 CrossRef Medline
55. Manjón JV, Coupé P, Buades A, et al. **MRI superresolution using self-similarity and image priors.** *Int J Biomed Imaging* 2010;2010:425891 CrossRef Medline
56. d'Arcy JA, Collins DJ, Rowland IJ, et al. **Applications of sliding window reconstruction with Cartesian sampling for dynamic contrast enhanced MRI.** *NMR Biomed* 2002;15:174–83 CrossRef Medline
57. Lustig M, Donoho D, Pauly JM. **Sparse MRI: the application of compressed sensing for rapid MR imaging.** *Magn Reson Med* 2007;58:1182–95 CrossRef Medline
58. Akkus Z, Galimzianova A, Hoogi A, et al. **Deep learning for brain MRI segmentation: state of the art and future directions.** *J Digit Imaging* 2017;30:449–59 CrossRef Medline
59. Zhang K, Zuo W, Chen Y, et al. **Beyond a Gaussian denoiser: residual learning of deep CNN for image denoising.** *IEEE Trans Image Process* 2017;26:3142–55 CrossRef Medline
60. Avants BB, Yushkevich P, Pluta J, et al. **The optimal template effect in hippocampus studies of diseased populations.** *Neuroimage* 2010;49:2457–66 CrossRef Medline
61. Xing Y, Sapuan A, Dineen RA, et al. **Life span pigmentation changes of the substantia nigra detected by neuromelanin-sensitive MRI.** *Mov Disord* 2018;33:1792–99 CrossRef Medline
62. Niemann K, van Nieuwenhofen I. **One atlas: three anatomies—relationships of the Schaltenbrand and Wahren microscopic data.** *Acta Neurochir (Wien)* 1999;141:1025–38 CrossRef Medline
63. Avants BB, Tustison NJ, Song G, et al. **A reproducible evaluation of ANTs similarity metric performance in brain image registration.** *Neuroimage* 2011;54:2033–44 CrossRef Medline
64. Wang H, Yushkevich P. **Multi-atlas segmentation with joint label fusion and corrective learning: an open source implementation.** *Front Neuroinform* 2013;7:27 CrossRef Medline
65. Lambert C, Chowdhury R, Fitzgerald TH, et al. **Characterizing aging in the human brainstem using quantitative multimodal MRI analysis.** *Front Hum Neurosci* 2013;7:462 CrossRef Medline
66. Nye JA, Purselle D, Plisson C, et al. **Decreased brainstem and putamen SERT binding potential in depressed suicide attempters using [11C]-zient PET imaging.** *Depress Anxiety* 2013;30:902–07 CrossRef Medline